

# Synergy between isolated Fe and Co sites accelerates oxygen evolution

Tianmi Tang<sup>1,§</sup>, Zhiyao Duan<sup>2,§</sup> (✉), Didar Baimanov<sup>3,4,§</sup>, Xue Bai<sup>1</sup>, Xinyu Liu<sup>5</sup>, Liming Wang<sup>3</sup>, Zhenlu Wang<sup>1</sup> (✉), and Jingqi Guan<sup>1</sup> (✉)

<sup>1</sup> Institute of Physical Chemistry, College of Chemistry, Jilin University, 2519 Jiefang Road, Changchun 130021, China

<sup>2</sup> State Key Laboratory of Solidification Processing, School of Materials Science and Engineering, Northwestern Polytechnical University, Xi'an 710072, China

<sup>3</sup> CAS Key Laboratory for Biomedical Effects of Nanomaterials and Nanosafety & CAS-HKU Joint Laboratory of Metallomics on Health and Environment, Institute of High Energy Physics, Chinese Academy of Sciences, Beijing 100049, China

<sup>4</sup> University of Chinese Academy of Sciences, Beijing 100049, China

<sup>5</sup> School of Physical Science and Technology, ShanghaiTech University, No.393 Middle Huaxia Road, Pudong New District, Shanghai 201210, China

<sup>§</sup> Tianmi Tang, Zhiyao Duan, and Didar Baimanov contributed equally to this work.

© Tsinghua University Press 2022

Received: 1 July 2022 / Revised: 30 August 2022 / Accepted: 1 September 2022

## ABSTRACT

Dual-metal catalysts with synergistic effect exhibit enormous potential for sustainable electrocatalytic applications and mechanism research. Compared with mono-metal-site catalysts, dual-metal-site catalysts exhibit higher efficiency for the oxygen evolution reaction (OER) due to reduced energy barrier of the process involving proton-coupled multi-electron transfer. Herein, we construct dual-metal Fe-Co sites coordinated with nitrogen in graphene (FeCo-NG), which exhibits high OER performance with onset overpotential of only 126 mV and Tafel slope of 120 mV·dec<sup>-1</sup>, showing that the rate-determining step is controlled by the single-electron transfer step. Theoretical calculations reveal that the FeN<sub>4</sub> site exhibits lower OER overpotential than the CoN<sub>4</sub> site due to appropriate adsorption energy of OOH\* on the former, while the O\* adsorbed on the adjacent Co site could stabilize the OOH\* on the FeN<sub>4</sub> site through hydrogen bond interaction.

## KEYWORDS

Co-N-C, Fe-N-C, oxygen evolution reaction, dual-atom catalysis, theoretical calculation

## 1 Introduction

The oxygen evolution reaction (OER) plays a conspicuous part in electrolytic water and electrochemical carbon dioxide reduction [1, 2]. Usually, a high overpotential (> 300 mV) should be applied in the anode to conquer the tardy OER kinetics, resulting in low energy utilization [3, 4]. Thereby, the development of cost-effective and high-performance OER catalysts has been getting increased attention [5–7]. In the last few decades, Co-Fe based catalysts, including oxides, oxyhydroxides, chalcogenides, nitrides, phosphides, and carbon-based composites [8, 9], showed high OER performance in alkaline media due to a cooperation mechanism between Co and Fe. Although many findings demonstrate that the coexistence of Co and Fe can greatly increase OER performance, the identification of the catalytically active centers in Co-Fe based electrocatalysts is still challenging [10, 11]. Therefore, different attitudes have been held regarding whether Co or Fe makes up the active centers.

Smith et al. used time-resolved *in situ* X-ray absorption spectroscopy (XAS) measurements to reveal that the OER took place primarily at di-μ-oxo bridged Co-Co and di-μ-oxo bridged Fe-Co sites on Fe-Co oxides [12]. Furthermore, Zhu et al. found that Co<sup>3+</sup> centers with oxygen vacancies favored the adsorption of

water molecules and the introduction of Fe<sup>3+</sup> can accelerate the oxidation of Co<sup>3+</sup> to Co<sup>4+</sup>, thus increasing OER activity [13]. However, Boettcher et al. used operando XAS measurements to reveal that the Fe species were partially oxidized and the Fe–O bond shortened during OER on the Co(Fe)O<sub>x</sub>H<sub>y</sub>, while the Co<sup>3+</sup> ions were not oxidized to higher valence state, suggesting that Fe species played a pivotal role in the OER [14]. Moreover, Yeo et al. used *in situ* XAS analysis to find that the coordination number of Fe sites decreased during OER and they proposed that Fe centers with oxygen vacancies should be the active sites on Fe<sup>3+</sup>/CoO<sub>x</sub> catalysts for water oxidation [15]. Although there is increasing evidence that iron might be the active center for the OER on Co-Fe-based oxides, the OER activity of FeO<sub>x</sub> is far lower than that of CoO<sub>x</sub> due to decreased strength of the OH<sub>ad</sub>–M<sup>n+</sup> interaction, implying that monometallic Fe-based oxyhydroxides are not excellent catalysts for the OER [16]. Therefore, iron element was frequently used as a dopant to improve the OER performance of Co- and Ni-based materials [8].

Recently, diatomic Fe-based electrocatalysts exhibited higher electrocatalytic performance than single-atom electrocatalysts for OER [17, 18], oxygen reduction reaction [18–20], CO<sub>2</sub> reduction [21, 22], and N<sub>2</sub> reduction [23, 24]. The well-defined atomic structure and tunable coordination configuration of single-atom

catalysts (SACs) gives us a better understanding of the catalytically active sites and the reaction mechanism on bimetallic Fe-based catalysts for the OER [25, 26]. For instance, Sun et al. found that N-coordinated Ni-Fe diatomic sites showed higher OER activity than monometal-doped counterparts [18]. Due to different adsorption energies toward OER intermediates on Fe and Ni sites,  $\text{OH}^*$  and  $\text{O}^*$  were adsorbed at Fe sites, while  $\text{OOH}^*$  was formed at Ni sites, which greatly reduced reaction energy barrier. Using *in situ* XAS measurements, Patzke et al. found that both Ni and Fe sites took part in the  $^*\text{OH}$  deprotonation process, and the O–O bond was formed at the Ni–O–Fe site on a dual-site NiFe SAC during the OER [27]. Hu et al. introduced 10 ppm  $\text{Fe}^{3+}$  into the KOH electrolyte and found that the OER performance of atomic Co–N–C can be greatly enhanced [17]. Using operando XAS analysis, they revealed that the formation of dual-metallic Co–O–Fe sites promoted the OER kinetics. As far as we are aware, direct fabrication of dual-atom Fe–Co catalysts and an in-depth understanding of the structure–function relationship of Fe and Co during OER have not been achieved in previous works. Moreover, the investigation of dual-site SACs for OER is still immature, and the fabrication of two kinds of metal ions with adjustable coordination environment on the same substrate remains challenging.

In this work, we fabricate atomically dispersed N-coordinated Fe–Co dual-sites onto N-doped graphene (FeCo-NG), which exhibits much higher OER activity than single-site catalysts. XAS measurements reveal that both Fe and Co ions are isolated and coordinated with four nitrogen atoms. Density functional theory (DFT) calculations reveal that dual-metal Fe–Co sites show lower OER overpotential than standalone  $\text{FeN}_4$  and  $\text{CoN}_4$  sites due to synergic action between adjacent Fe and Co sites.

## 2 Results and discussion

### 2.1 Structural characterization

The synthetic procedure of FeCo-NG is schematically demonstrated in Fig. 1(a).  $\text{Fe}^{3+}/\text{GO}$  (GO: graphene oxide),  $\text{Co}^{2+}/\text{GO}$ , and  $\text{Fe}^{3+}\text{--Co}^{2+}/\text{GO}$  precursors were mixed with urea and annealed in  $\text{N}_2$  to obtain Fe-NG, Co-NG, and FeCo-NG, respectively. Without urea, the obtained product was nominated as Fe-G, Co-G, and FeCo-G, respectively. From the X-ray diffraction (XRD) patterns (Fig. S1 in the Electronic Supplementary Material (ESM)), no obvious peaks due to Fe/Co-based nanoparticles can be found, indicating that the Fe/Co-based species were highly dispersed onto the graphene (G) or N-doped graphene (NG) supports. Moreover, the peak at  $25.6^\circ$  in the graphene is shifted to  $26.6^\circ$  after N-doping, suggesting that N-doping can modulate the structure of graphene [28, 29]. Furthermore, after doping Fe and Co into G and NG, this peak becomes much weaker, implying that Fe and Co ions were successfully immobilized into the lattice structure [18, 30]. The high-angle annular dark-field scanning transmission electron microscopy (HAADF-STEM) images further verify that no obvious Fe/Co-based nanoparticles were formed on the NG support (Fig. 1(b)) and Fe/Co ions were atomically dispersed (Fig. 1(c)). From the EDX mappings, Fe, Co, and N species are uniformly dispersed onto the graphene support (Figs. S2 and S3 in the ESM). The mass loadings of Fe and Co in the FeCo-NG are both ca. 1.2 wt.% as determined by inductively coupled plasma-atomic emission spectroscopy (ICP-AES) measurements.

The surface composition and elemental state of FeCo-NG were analyzed by X-ray photoemission spectroscopy (XPS). The survey spectrum indicates the co-existence of C, N, O, Fe, and Co elements (Fig. S4 in the ESM). The Fe  $2p_{3/2}$  and Fe  $2p_{1/2}$  are

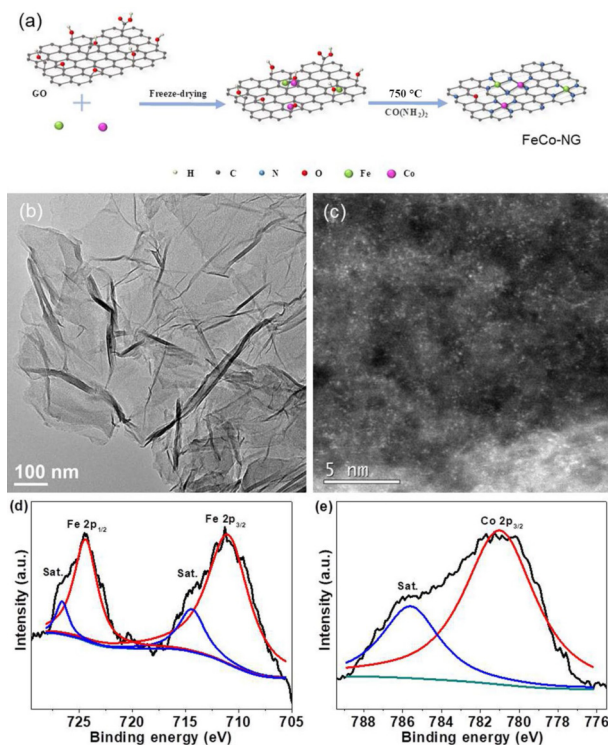


**Figure 1** (a) Schematic of the synthetic process of FeCo-NG. (b) and (c) HAADF images, (d) Fe 2p XPS spectrum, and (e) Co 2p XPS spectrum.

centered at 711.0 and 724.4 eV, respectively (Fig. 1(d)), illustrating that the dominant oxidation state of Fe is +2 valence [31]. The Co  $2p_{3/2}$  is centered at 781.0 eV (Fig. 1(e)), characteristic of  $\text{Co}^{2+}$  [32]. The N 1s spectrum can be deconvoluted into five typical peaks at 398.0, 398.6, 400.2, 401.0, and 402.5 eV, attributed to pyridinic-N, Fe/Co- $\text{N}_x$ , pyrrolic-N, graphitic-N, and oxidized-N, respectively [27, 33]. To further identify the local structures and oxidation states of Fe and Co ions in the FeCo-NG, Ni, XAS measurements were performed. The absorption Fe K-edge of FeCo-NG is located between Fe foil and  $\text{Fe}_2\text{O}_3$  and almost overlaps with FePc (Fig. 2(a)), indicating that the average valence state of Fe species is  $\text{Fe}^{2+}$  in agreement with the XPS results. The coordination environments of the Fe and Co ions in the FeCo-NG are compared with FePc and CoPc in the K range (Fig. S5 in the ESM), respectively, showing similar coordination environments, which suggests that the Fe and Co ions in the FeCo-NG might coordinate with nitrogen atoms. The Fourier-transform extended X-ray absorption fine structure (FT-EXAFS) spectrum at Fe K-edge of FeCo-NG exhibits a main peak located at around 1.78 Å (Fig. 2(b)), which can be ascribed to Fe–N/O bond [34]. The fitted FT-EXAFS spectrum exhibits that the bond length of Fe–N coordination is  $1.99 \pm 0.02$  Å and the coordination number is  $4.6 \pm 0.7$  (Fig. 2(c) and Table S1 in the ESM). Similarly, the absorption Co K-edge of FeCo-NG is very close to that of CoPc, but far away from those of Co foil and  $\text{Co}_3\text{O}_4$  (Fig. 2(d)), indicating that the average valence state of Co species is  $\text{Co}^{2+}$  in agreement with the aforementioned XPS results. The FT-EXAFS spectrum at Co K-edge of FeCo-NG illustrates a main peak located at around 1.67 Å (Fig. 2(e)), which can be attributed to Co–N/O bond. The fitted FT-EXAFS spectrum shows that the bond length of the Co–N coordination is  $1.88 \pm 0.03$  Å and its coordination number is  $4.1 \pm 0.4$  (Fig. 2(f) and Table S1 in the ESM).

### 2.2 Electrocatalytic OER performance

The electrocatalytic OER performance of the FeCo-NG was measured in 1 M KOH solution. For comparison, the catalytic

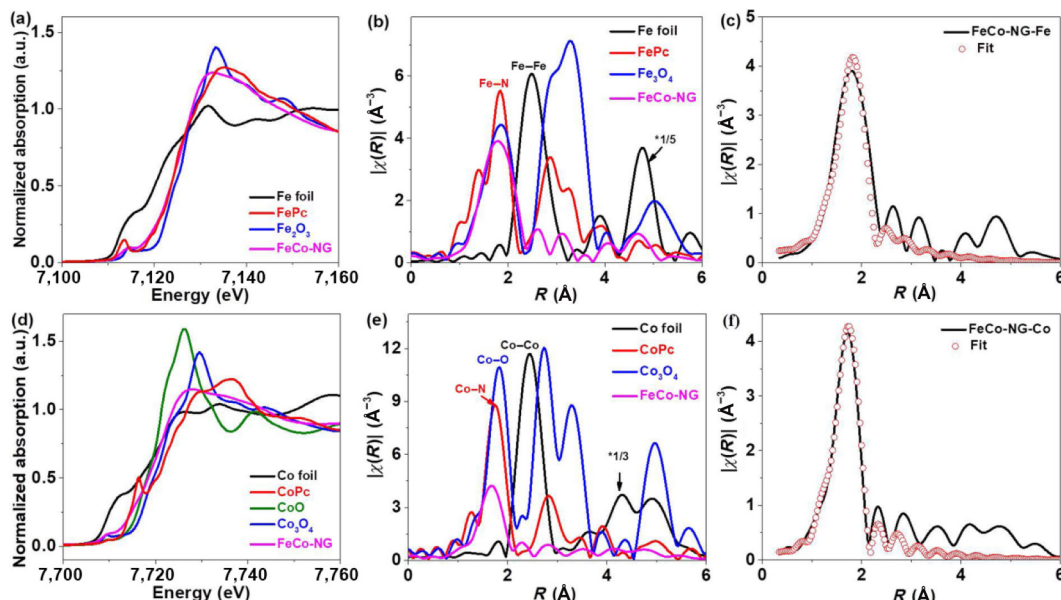


**Figure 2** (a) XANES spectra at Fe K-edge of FeCo-NG and referred samples. (b) EXAFS spectra at Fe K-edge. (c) FT-EXAFS fitting spectrum at Fe K-edge of FeCo-NG. (d) XANES spectra at Co K-edge of FeCo-NG and referred samples. (e) EXAFS spectra at Co K-edge. (f) FT-EXAFS fitting spectrum at Co K-edge of FeCo-NG.

OER performance of Fe-G, Fe-NG, Co-G, Co-NG, FeCo-G, and RuO<sub>2</sub> was also studied. The OER activity of isolated single-atom Fe/Co sites can be significantly improved by N-coordination (Fig. 3(a)). For example, the overpotential ( $\eta_{10}$ ) at 10 mA·cm<sup>-2</sup> for Fe-NG, Co-NG, and FeCo-NG is 422, 408, and 276 mV, respectively, which is much lower than that for N-free Fe-G (574 mV), Co-G (468 mV), and FeCo-G (370 mV). The Tafel slope of FeCo-NG is measured as 120 mV·dec<sup>-1</sup> (Fig. 3(b)), close to that of Co-G (113 mV·dec<sup>-1</sup>), FeCo-G (137 mV dec<sup>-1</sup>), and RuO<sub>2</sub> (110 mV·dec<sup>-1</sup>), implying that the OER is controlled by the single-electron transfer step [35, 36]. Since the Tafel of FeCo-NG is obviously different from that of Fe-NG (91 mV·dec<sup>-1</sup>) and Co-NG (85 mV·dec<sup>-1</sup>), a different reaction kinetics may occur between them. The FeCo-NG exhibits better OER performance than commercial RuO<sub>2</sub> ( $\eta_{10}$  = 352 mV) and most state-of-the-art N-doped FeCo-based materials reported recently (Fig. 3(c)), such as Fe/Co double hydroxide/oxide nanoparticles on N-doped CNTs (FeCo-DHO/NCNTs,  $\eta_{10}$  = 320 mV) [37], Fe-Co nanoparticles on N-doped carbon (Co<sub>3</sub>Fe<sub>0.8</sub>N,  $\eta_{10}$  = 318 mV) [38], N and Fe codoped CoO nanoparticles (Co<sub>0.89</sub>Fe<sub>0.11</sub>O-N,  $\eta_{10}$  = 304 mV) [39], metal-organic-framework-derived Fe-Co-O/Co metal@N-doped carbon on Ni foam (Fe-Co-O/Co@NC/NF,  $\eta_{10}$  = 299 mV) [40], carbon aerogels containing Fe-Co bimetal sites (NCAG/Fe-Co,  $\eta_{10}$  = 293 mV) [41], cobalt-iron nitrides on N-doped multi-walled carbon nanotubes (Co-Fe-N@MWCNT,  $\eta_{10}$  = 290 mV) [42], highly-dispersed Fe/Co/N on graphene (FeCoN-Gs,  $\eta_{10}$  = 288 mV) [43], and Fe-Co anchored on N-doped porous carbon (Fe-Co/NC-800,  $\eta_{10}$  = 279 mV) [44].

The influence of annealing temperature on the OER performance of FeCo-NG was investigated (Fig. 3(d)). The OER activity increases with raising the annealing temperature and achieves the best effect at 750 °C. Further increasing the annealing temperature results in worse catalytic performance, implying that the annealing temperature will influence the coordination structure of isolated single-atom Fe and Co and therefore affect the electrocatalytic activity [45]. In addition, we investigated the influence of Fe-doping content in the FeCo-NG on the OER performance (Fig. S6 in the ESM). With increasing the Fe-doping content, the OER performance can be gradually increased and reaches a maximum when the initial Fe-doping content is 0.6 wt.%. Further increasing the Fe-doping content would result in the decrease in OER activity due to the agglomeration of metal species during the annealing process.

To compare available active sites on various catalysts for the OER, the electrochemically active surface area (ECSA) was measured by calculating from the electrochemical double-layer capacitance (Figs. S7–S12 in the ESM). For Fe-G, Fe-NG, Co-G, Co-NG, FeCo-G, and FeCo-NG, the ECSA is 15.4, 46.9, 122.5, 186.5, 281.8, and 340.7 cm<sup>2</sup>, respectively. The order of the ECSA agrees with the order of the electrocatalytic activity obtained by the linear sweep voltammetry (LSV) measurement. The N-doping can vastly enhance active sites, thus improving OER activity. Moreover, dual-metal doping can also increase active sites due to a cooperation mechanism, thus enhancing catalytic performance. To further study the OER kinetics, electrochemical impedance spectroscopy (EIS) spectra of various samples were conducted (Fig. 3(e)). The charge-transfer resistance ( $R_{ct}$ ) for the Fe-G, Fe-NG, Co-G, Co-NG, FeCo-G, and FeCo-NG is measured to be 465, 186, 63, 33, 65, and 24  $\Omega$  cm<sup>2</sup>, respectively. As expected, Fe-G shows the largest  $R_{ct}$ . Introduction of N dopant and/or Co element can dramatically decrease the  $R_{ct}$ , and Co/N-codoped into the Fe-based system exhibits the lowest  $R_{ct}$ , which is favorable for the OER process.

The OER stability of FeCo-NG was tested via the chronoamperometry at a constant potential for 15 h (Fig. 3(f)). The FeCo-NG exhibits a small degradation of 6.6% after continuous testing for the OER, indicating excellent electrocatalytic stability. The metal valence state of FeCo-NG after OER testing was analyzed by XPS (Fig. S13 in the ESM). Partial Fe<sup>2+</sup> and Co<sup>2+</sup> were oxidized to Fe<sup>3+</sup> and Co<sup>3+</sup> during OER due to the formation of FeN<sub>4</sub>-OH and CoN<sub>4</sub>-OH species, which should be key intermediates for the reaction as revealed by the following theoretical calculations.

### 2.3 DFT calculations

To rationalize the enhancement of OER activity in FeCo-NG, we performed first-principles DFT calculations to illustrate the effects of dual-metal sites in enhancing OER reactivity. We proposed the active site in the FeCo-NG catalyst to be separate single CoN<sub>4</sub> and FeN<sub>4</sub> in adjacent as shown in Fig. 4 since the XAFS results only show Fe/Co-N<sub>4</sub> coordination without Fe-Co coordination. We searched for optimal spin states for both Co and Fe centers. It is shown that the FeN<sub>4</sub> center possesses the intermediate spin state, while the CoN<sub>4</sub> center possesses the low spin state. The detailed d-orbital configurations for the FeN<sub>4</sub> and CoN<sub>4</sub> centers in the dual

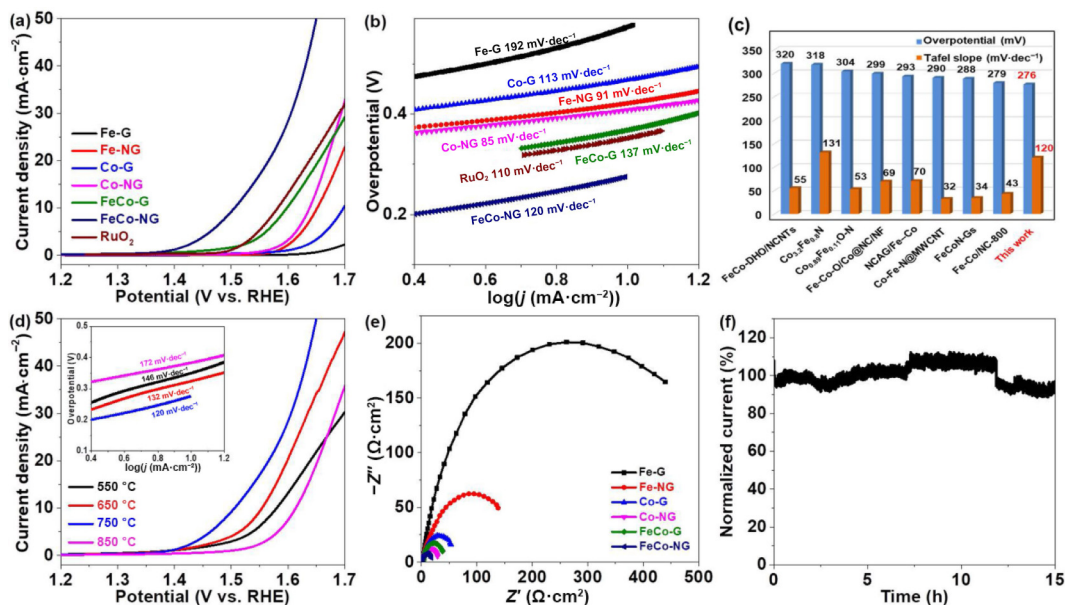


**Figure 3** (a) OER polarization curves of Fe-G, Fe-NG, Co-G, Co-NG, FeCo-G, FeCo-NG, and commercial RuO<sub>2</sub>. (b) Tafel slopes and (c) comparison of overpotentials at 10 mA·cm<sup>-2</sup> and Tafel slopes. (d) Influence of annealing temperature on the OER performance of FeCo-NG (inset: Tafel slopes). (e) Nyquist plots and (f) chronoamperometric response of FeCo-NG.

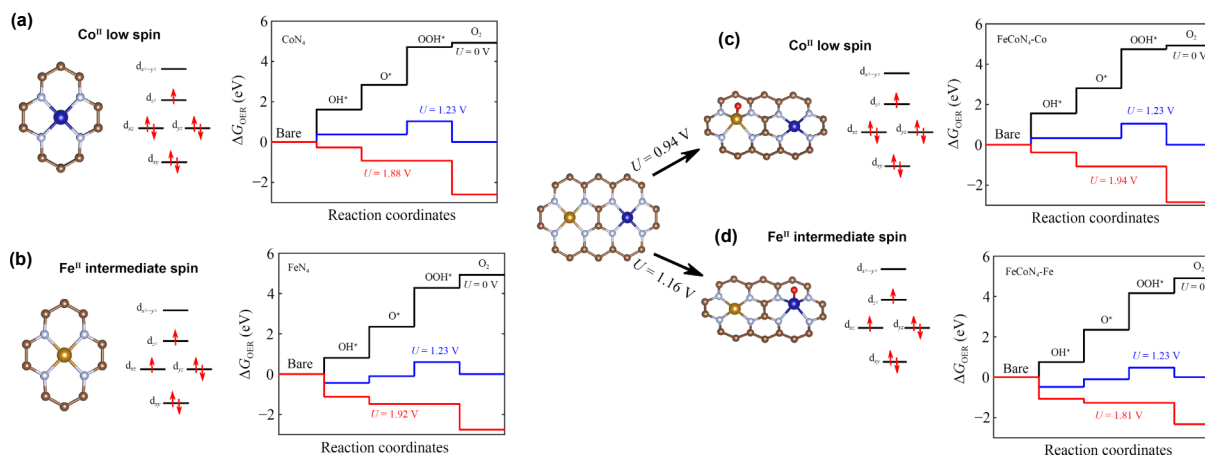


**Figure 4** Atomic structures, spin states, and free energy diagrams (FEDs) of OER on various catalytic site: (a) CoN<sub>4</sub> site, (b) FeN<sub>4</sub> site, (c) FeN<sub>4</sub>O-CoN<sub>4</sub> site, and (d) FeN<sub>4</sub>-CoON<sub>4</sub> site.

FeN<sub>4</sub>-CoN<sub>4</sub> model are shown in Figs. 4(c) and 4(d). It should be noticed that the spin states of Fe and Co centers in the dual FeN<sub>4</sub>-CoN<sub>4</sub> model do not shift as compared to single CoN<sub>4</sub> and FeN<sub>4</sub> sites. The Fe-N and Co-N bond lengths are 1.91 and 1.88 Å, respectively, which are close to the EXAFS fitting results. We employed DFT + *U* method to evaluate the theoretical OER overpotentials ( $\eta_{\text{OER}}$ ) on Fe and Co sites in the dual FeN<sub>4</sub>-CoN<sub>4</sub> model and compared with standalone FeN<sub>4</sub> and CoN<sub>4</sub> sites. Under OER conditions, the Fe and Co centers are oxidized because of high anodic potential. It is calculated that the FeN<sub>4</sub> site is oxidized to FeON<sub>4</sub> at  $U = 0.94$  V, while the CoN<sub>4</sub> site can be oxidized at a higher potential of  $U = 1.16$  V. Consequently, we set one of the dual sites oxidized when we examine the OER activity of the other site. Based on the model, we calculated the binding energies of OER intermediates and then evaluated  $\eta_{\text{OER}}$ . The CoN<sub>4</sub> site has an  $\eta_{\text{OER}}$  of 0.61 V due to the relatively weak adsorption of OOH\* (Fig. 4(c)). Comparing to the standalone CoN<sub>4</sub>, the overpotential is increased by 0.06 V because higher gap between O\* and OOH\* ( $\Delta G_{\text{O}} - \Delta G_{\text{OOH}}$ ). The FeN<sub>4</sub> site has an  $\eta_{\text{OER}}$  of 0.58 V with the potential-limiting step being the O\* to OOH\* step due to relatively strong adsorption of O\* (Fig. 4(d)). The overpotential is lower than standalone FeN<sub>4</sub> site due to stabilized adsorption of OOH\*, which lowers the gap between O\* and OOH\*. The

stabilization of OOH\* is attributed to the attractive hydrogen bond between O\* adsorbed on Co and OOH\* on Fe. We purposely turned the OOH\* on FeN<sub>4</sub> away from the adsorbed O\* by 180° and recalculated the adsorption energy of OOH\* (Fig. S14 in the ESM). It turns out that the OOH\* adsorption is destabilized by 0.1 eV, which demonstrates the role of hydrogen bonding in OOH\* stabilization. Overall, we have demonstrated that the FeN<sub>4</sub> in the dual model has the lowest OER overpotential because of the stabilization of OOH\* as a result of attractive hydrogen bonding between the adjacent Co and Fe sites.

### 3 Conclusions

In summary, we have successfully fabricated atomically dispersed dual-metal Fe-Co sites embedded onto N-doped graphene by one step process. The FeCo-NG exhibited excellent OER performance with low overpotential of 276 mV, over which the reaction is controlled by the single-electron transfer step. Structure characterizations showed that Fe and Co are both coordinated with four nitrogen atoms. DFT calculations revealed that the OER might mainly take place on the FeN<sub>4</sub> site due to appropriate adsorption of OOH\* intermediate, while O\* adsorbed on the adjacent Co site could stabilize the OOH\* through hydrogen bond interaction.

## Acknowledgements

This work was supported by the National Natural Science Foundation of China (Nos. 22075099 and 31971322), the Education Department of Jilin Province (Nos. JJKH20220967KJ and JJKH20220968CY), the Natural Science Foundation of Jilin Province (No. 20220101051JC), the Natural Science Foundation of Shaanxi Province (No. D5110220052), the Fundamental Research Funds for the Central Universities (No. D5000210743), and Beijing Municipal Health Commission (No. 2021-1G-1191).

**Electronic Supplementary Material:** Supplementary material (XRD, TEM, scanning electron microscopy (SEM), XPS, and electrochemical measurements) is available in the online version of this article at <https://doi.org/10.1007/s12274-022-5001-3>.

## References

- [1] Guan, J. Q.; Bai, X.; Tang, T. M. Recent progress and prospect of carbon-free single-site catalysts for the hydrogen and oxygen evolution reactions. *Nano Res.* **2022**, *15*, 818–837.
- [2] Tang, T. M.; Li, S. S.; Sun, J. R.; Wang, Z. L.; Guan, J. Q. Advances and challenges in two-dimensional materials for oxygen evolution. *Nano Res.*, in press, <https://doi.org/10.1007/s12274-022-4575-0>.
- [3] Zhang, Q. Q.; Guan, J. Q. Atomically dispersed catalysts for hydrogen/oxygen evolution reactions and overall water splitting. *J. Power Sources* **2020**, *471*, 228446.
- [4] Zheng, X. B.; Chen, Y. P.; Lai, W. H.; Li, P.; Ye, C. L.; Liu, N. N.; Dou, S. X.; Pan, H. G.; Sun, W. P. Enriched d-band holes enabling fast oxygen evolution kinetics on atomic-layered defect-rich lithium cobalt oxide nanosheets. *Adv. Funct. Mater.* **2022**, *32*, 2200663.
- [5] Zhang, Q. Q.; Guan, J. Q. Applications of single-atom catalysts. *Nano Res.* **2022**, *15*, 38–70.
- [6] Tang, T. M.; Wang, Z. L.; Guan, J. Q. A review of defect engineering in two-dimensional materials for electrocatalytic hydrogen evolution reaction. *Chin. J. Catal.* **2022**, *43*, 636–678.
- [7] Bai, X.; Wang, L. M.; Nan, B.; Tang, T. M.; Niu, X. D.; Guan, J. Q. Atomic manganese coordinated to nitrogen and sulfur for oxygen evolution. *Nano Res.* **2022**, *15*, 6019–6025.
- [8] Anantharaj, S.; Kundu, S.; Noda, S. “The Fe Effect”: A review unveiling the critical roles of Fe in enhancing OER activity of Ni and Co based catalysts. *Nano Energy* **2021**, *80*, 105514.
- [9] Han, L.; Dong, S. J.; Wang, E. K. Transition-metal (Co, Ni, and Fe)-based electrocatalysts for the water oxidation reaction. *Adv. Mater.* **2016**, *28*, 9266–9291.
- [10] Sultan, S.; Tiwari, J. N.; Singh, A. N.; Zhumagali, S.; Ha, M. R.; Myung, C. W.; Thangavel, P.; Kim, K. S. Single atoms and clusters based nanomaterials for hydrogen evolution, oxygen evolution reactions, and full water splitting. *Adv. Energy Mater.* **2019**, *9*, 1900624.
- [11] Bai, X.; Duan, Z. Y.; Nan, B.; Wang, L. M.; Tang, T. M.; Guan, J. Q. Unveiling the active sites of ultrathin Co-Fe layered double hydroxides for the oxygen evolution reaction. *Chin. J. Catal.* **2022**, *43*, 2240–2248.
- [12] Smith, R. D. L.; Pasquini, C.; Loos, S.; Chernev, P.; Klingan, K.; Kubella, P.; Mohammadi, M. R.; Gonzalez-Flores, D.; Dau, H. Spectroscopic identification of active sites for the oxygen evolution reaction on iron-cobalt oxides. *Nat. Commun.* **2017**, *8*, 2022.
- [13] Zhuang, L. Z.; Ge, L.; Yang, Y. S.; Li, M. R.; Jia, Y.; Yao, X. D.; Zhu, Z. H. Ultrathin iron-cobalt oxide nanosheets with abundant oxygen vacancies for the oxygen evolution reaction. *Adv. Mater.* **2017**, *29*, 1606793.
- [14] Enman, L. J.; Stevens, M. B.; Dahan, M. H.; Nellist, M. R.; Toroker, M. C.; Boettcher, S. W. Operando X-ray absorption spectroscopy shows iron oxidation is concurrent with oxygen evolution in cobalt-iron (oxy)hydroxide electrocatalysts. *Angew. Chem., Int. Ed.* **2018**, *57*, 12840–12844.
- [15] Gong, L.; Chng, X. Y. E.; Du, Y. H.; Xi, S. B.; Yeo, B. S. Enhanced catalysis of the electrochemical oxygen evolution reaction by iron(III) ions adsorbed on amorphous cobalt oxide. *ACS Catal.* **2018**, *8*, 807–814.
- [16] Subbaraman, R.; Tripkovic, D.; Chang, K. C.; Strmcnik, D.; Paulikas, A. P.; Hirunsit, P.; Chan, M.; Greeley, J.; Stamenkovic, V.; Markovic, N. M. Trends in activity for the water electrolyser reactions on 3d M(Ni, Co, Fe, Mn) hydr(oxy)oxide catalysts. *Nat. Mater.* **2012**, *11*, 550–557.
- [17] Bai, L. C.; Hsu, C. S.; Alexander, D. T. L.; Chen, H. M.; Hu, X. L. A cobalt-iron double-atom catalyst for the oxygen evolution reaction. *J. Am. Chem. Soc.* **2019**, *141*, 14190–14199.
- [18] Wu, C. C.; Zhang, X. M.; Xia, Z. X.; Shu, M.; Li, H. Q.; Xu, X. L.; Si, R.; Rykov, A. I.; Wang, J. H.; Yu, S. S. et al. Insight into the role of Ni-Fe dual sites in the oxygen evolution reaction based on atomically metal-doped polymeric carbon nitride. *J. Mater. Chem. A* **2019**, *7*, 14001–14010.
- [19] Zhao, X. M.; Liu, X.; Huang, B. Y.; Wang, P.; Pei, Y. Hydroxyl group modification improves the electrocatalytic ORR and OER activity of graphene supported single and bi-metal atomic catalysts (Ni, Co, and Fe). *J. Mater. Chem. A* **2019**, *7*, 24583–24593.
- [20] Zhang, Q. Q.; Guan, J. Q. Applications of atomically dispersed oxygen reduction catalysts in fuel cells and zinc-air batteries. *Energy Environ. Mater.* **2021**, *4*, 307–335.
- [21] Tang, T. M.; Wang, Z. L.; Guan, J. Q. Optimizing the electrocatalytic selectivity of carbon dioxide reduction reaction by regulating the electronic structure of single-atom M-N-C materials. *Adv. Funct. Mater.* **2022**, *32*, 2111504.
- [22] Jing, H. Y.; Zhu, P.; Zheng, X. B.; Zhang, Z. D.; Wang, D. S.; Li, Y. D. Theory-oriented screening and discovery of advanced energy transformation materials in electrocatalysis. *Adv. Powder Mater.* **2022**, *1*, 100013.
- [23] Wang, X. W.; Qiu, S. Y.; Feng, J. M.; Tong, Y. Y.; Zhou, F. L.; Li, Q. Y.; Song, L.; Chen, S. M.; Wu, K. H.; Su, P. P. et al. Confined Fe-Cu clusters as sub-nanometer reactors for efficiently regulating the electrochemical nitrogen reduction reaction. *Adv. Mater.* **2020**, *32*, 2004382.
- [24] Zheng, X. B.; Li, B. B.; Wang, Q. S.; Wang, D. S.; Li, Y. D. Emerging low-nuclearity supported metal catalysts with atomic level precision for efficient heterogeneous catalysis. *Nano Res.* **2022**, *15*, 7806–7839.
- [25] Zheng, X. B.; Yang, J. R.; Xu, Z. F.; Wang, Q. S.; Wu, J. B.; Zhang, E. H.; Dou, S. X.; Sun, W. P.; Wang, D. S.; Li, Y. D. Ru-Co pair sites catalyst boosts the energetics for the oxygen evolution reaction. *Angew. Chem., Int. Ed.* **2022**, *134*, e202205946.
- [26] Han, J. Y.; Zhang, M. Z.; Bai, X.; Duan, Z. Y.; Tang, T. M.; Guan, J. Q. Mesoporous Mn-Fe oxyhydroxides for oxygen evolution. *Inorg. Chem. Front.* **2022**, *9*, 3559–3565.
- [27] Wan, W. C.; Zhao, Y. G.; Wei, S. Q.; Triana, C. A.; Li, J. G.; Arcifa, A.; Allen, C. S.; Cao, R.; Patzke, G. R. Mechanistic insight into the active centers of single/dual-atom Ni/Fe-based oxygen electrocatalysts. *Nat. Commun.* **2021**, *12*, 5589.
- [28] Nechiyil, D.; Vinayan, B. P.; Ramaprabhu, S. Tri-iodide reduction activity of ultra-small size PtFe nanoparticles supported nitrogen-doped graphene as counter electrode for dye-sensitized solar cell. *J. Colloid Interface Sci.* **2017**, *488*, 309–316.
- [29] Ma, L. T.; Chen, S. M.; Pei, Z. X.; Huang, Y.; Liang, G. J.; Mo, F. N.; Yang, Q.; Su, J.; Gao, Y. H.; Zapien, J. A. et al. Single-site active iron-based bifunctional oxygen catalyst for a compressible and rechargeable zinc-air battery. *ACS Nano* **2018**, *12*, 1949–1958.
- [30] Zhao, S. Y.; Zhang, L. J.; Johannessen, B.; Saunders, M.; Liu, C.; Yang, S. Z.; Jiang, S. P. Designed iron single atom catalysts for highly efficient oxygen reduction reaction in alkaline and acid media. *Adv. Mater. Interfaces* **2021**, *8*, 2001788.
- [31] Guo, X. M.; Liu, S. J.; Wan, X. H.; Zhang, J. H.; Liu, Y. J.; Zheng, X. J.; Kong, Q. H.; Jin, Z. Controllable solid-phase fabrication of an Fe<sub>2</sub>O<sub>3</sub>/Fe<sub>3</sub>C<sub>2</sub>/Fe-N-C electrocatalyst toward optimizing the oxygen reduction reaction in zinc-air batteries. *Nano Lett.* **2022**, *22*, 4879–4887.
- [32] Li, F.; Qin, T. T.; Sun, Y. P.; Jiang, R. J.; Yuan, J. F.; Liu, X. Q.; O'Mullane, A. P. Preparation of a one-dimensional hierarchical MnO@CNT@Co-N/C ternary nanostructure as a high-performance bifunctional electrocatalyst for rechargeable Zn-air batteries. *J. Mater. Chem. A* **2021**, *9*, 22533–22543.

- [33] Guan, J. Q.; Duan, Z. Y.; Zhang, F. X.; Kelly, S. D.; Si, R.; Dupuis, M.; Huang, Q. G.; Chen, J. Q.; Tang, C. H.; Li, C. Water oxidation on a mononuclear manganese heterogeneous catalyst. *Nat. Catal.* **2018**, *1*, 870–877.
- [34] Li, J. K.; Jiao, L.; Wegener, E.; Richard, L. L.; Liu, E. S.; Zitolo, A.; Sougrati, M. T.; Mukerjee, S.; Zhao, Z. P.; Huang, Y. et al. Evolution pathway from iron compounds to Fe<sub>1</sub>(II)-N<sub>4</sub> sites through gas-phase iron during pyrolysis. *J. Am. Chem. Soc.* **2020**, *142*, 1417–1423.
- [35] Suen, N. T.; Hung, S. F.; Quan, Q.; Zhang, N.; Xu, Y. J.; Chen, H. M. Electrocatalysis for the oxygen evolution reaction: Recent development and future perspectives. *Chem. Soc. Rev.* **2017**, *46*, 337–365.
- [36] Shen, T.; Huang, X. X.; Xi, S. B.; Li, W.; Sun, S. N.; Hou, Y. L. The ORR electron transfer kinetics control via Co-N<sub>x</sub> and graphitic N sites in cobalt single atom catalysts in alkaline and acidic media. *J. Energy Chem.* **2022**, *68*, 184–194.
- [37] Wu, M. J.; Wei, Q. L.; Zhang, G. X.; Qiao, J. L.; Wu, M. X.; Zhang, J. H.; Gong, Q. J.; Sun, S. H. Fe/Co double hydroxide/oxide nanoparticles on N-doped CNTs as highly efficient electrocatalyst for rechargeable liquid and quasi-solid-state zinc-air batteries. *Adv. Energy Mater.* **2018**, *8*, 1801836.
- [38] Zhang, K. K.; Mai, W. S.; Li, J.; Li, G. Q.; Tian, L. H.; Hu, W. Bimetallic Co<sub>3</sub>Fe<sub>0.8</sub>N-nitrogen-carbon nanocomposites for simultaneous electrocatalytic oxygen reduction, oxygen evolution, and hydrogen evolution. *ACS Appl. Nano Mater.* **2019**, *2*, 5931–5941.
- [39] Du, Q. G.; Su, P. P.; Cao, Z. Z.; Yang, J.; Price, C. A. H.; Liu, J. Construction of N and Fe co-doped CoO/Co<sub>x</sub>N interface for excellent OER performance. *Sustainable Mater. Technol.* **2021**, *29*, e00293.
- [40] Singh, T. I.; Rajeshkhanna, G.; Pan, U. N.; Kshetri, T.; Lin, H.; Kim, N. H.; Lee, J. H. Alkaline water splitting enhancement by MOF-derived Fe-Co-oxide/Co@NC-mNS heterostructure: Boosting OER and HER through defect engineering and *in situ* oxidation. *Small* **2021**, *17*, 2101312.
- [41] Chen, Y.; Hu, S. Q.; Nichols, F.; Bridges, F.; Kan, S. T.; He, T.; Zhang, Y.; Chen, S. W. Carbon aerogels with atomic dispersion of binary iron-cobalt sites as effective oxygen catalysts for flexible zinc-air batteries. *J. Mater. Chem. A* **2020**, *8*, 11649–11655.
- [42] Gao, T. T.; Jin, Z. Y.; Zhang, Y. J.; Tan, G. Q.; Yuan, H. Y.; Xiao, D. Coupling cobalt-iron bimetallic nitrides and N-doped multi-walled carbon nanotubes as high-performance bifunctional catalysts for oxygen evolution and reduction reaction. *Electrochim. Acta* **2017**, *258*, 51–60.
- [43] Wang, W. G.; Babu, D. D.; Huang, Y. Y.; Lv, J. Q.; Wang, Y. B.; Wu, M. X. Atomic dispersion of Fe/Co/N on graphene by ball-milling for efficient oxygen evolution reaction. *Int. J. Hydrogen Energy* **2018**, *43*, 10351–10358.
- [44] Tan, W.; Xie, S. Q.; Yang, J. W.; Lv, J. G.; Yin, J. F.; Zhang, C.; Wang, J. Y.; Shen, X. Y.; Zhao, M.; Zhang, M. et al. Effect of carbonization temperature on electrocatalytic water splitting of Fe-Co anchored on N-doped porous carbon. *J. Solid State Chem.* **2021**, *302*, 122435.
- [45] Yin, P. Q.; Yao, T.; Wu, Y. E.; Zheng, L. R.; Lin, Y.; Liu, W.; Ju, H. X.; Zhu, J. F.; Hong, X.; Deng, Z. X. et al. Single cobalt atoms with precise N-coordination as superior oxygen reduction reaction catalysts. *Angew. Chem., Int. Ed.* **2016**, *55*, 10800–10805.